Available online at www.sciencedirect.com
ScienceDirect
Physics Procedia 00 (2010) 1–10
Physics Procedia

A Novel Experiment to Search for the Decay $\mu \to eee$

André Schöning, Sebastian Bachmann and Rohin Narayan

Institute of Physics, University of Heidelberg, Philosophenweg 12, 69120 Heidelberg, Germany

Abstract

Design studies for an experiment searching for the lepton flavor violating decay $\mu \to eee$ are presented. The detector concept is based on thin layers of silicon sensors with fast readout. The aim of this experiment is to reach a sensitivity of $B(\mu \to eee) \approx 10^{-16}$ corresponding to an improvement by a factor 10000 compared to previous experiments.

Keywords: LFV, lepton flavor, muon decay, pixel sensor, MAPS
PACS: 13.35.Bv, 11.30.Fs, 12.15.Ff, 29.40.Wk, 29.40.Mc

1. Introduction

After the observation of lepton mixing through neutrino oscillations the discovery of lepton flavor violation in the charged lepton sector is still lacking. The exact mechanism of lepton flavor violation (LFV) and the size of this effect being unknown, the study of LFV is of big interest as it is connected to neutrino mass generation, CP violation and new physics beyond the Standard Model (SM). Sizable effects of LFV interactions are expected from supersymmetric models, Leptoquarks, or models with an extended Higgs sector (e.g. Higgs triplets).

Several experiments have been performed or are in operation to measure directly LFV using muons or taus. Most prominent is the search for the radiative muon decay $\mu \to e\gamma$ [1, 2, 3, 4], the decay $\mu \to eee$ [5] or the conversion of muons to electrons [6]. Recently several new limits on LFV processes with tau leptons were obtained [7, 8].

In this talk a new experiment for the search of the decay $\mu \to eee$ is proposed aiming for a sensitivity of $B(\mu \to eee)=10^{-16}$. This experiment could be performed at upgraded or new beam lines at the proton cyclotron at the Paul-Scherrer Institute (Switzerland) and would enhance the discovery potential by four orders of magnitude compared to the existing obtained by the Sindrum experiment [5] of $B(\mu \to eee) < 1.0 \times 10^{12}$.

LFV reactions are forbidden in the SM at tree level and can only be induced by lepton mixing through higher order loop diagrams. However, the neutrino mixing loop diagram, see figure 1 a), is largely suppressed resulting in tiny branching ratios for LFV decays of muons and taus $B \ll 10^{-50}$, thus giving high sensitivity to LFV reactions in models beyond the SM. Furthermore, LFV effects from new particles at the TeV scale are in many models naturally generated and are therefore considered to be a prominent signature for new physics. Figure 1 b) is shown as an example where supersymmetric particles run in a loop. Also new bosons (Higgs, Z') can mediate LFV four-fermion interactions as shown in figure 1 c).

The search for the decay $B(\mu \to eee)$ is sensitive to both, LFV loop and four-fermion interactions, and is complementary to other LFV muon decay channels as will be discussed in the next section.

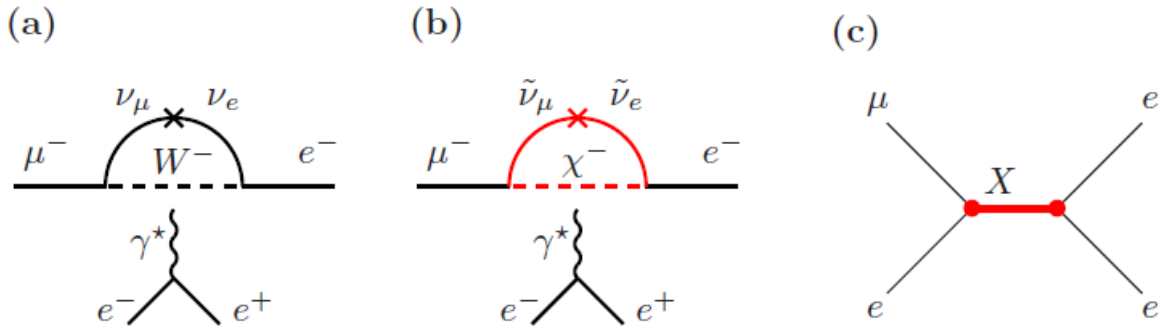

Figure 1: (a) loop diagram with SM neutrino mixing; (b) loop diagram with supersymmetric particles; (c) tree diagram with an intermediate boson.

2. Effective LFV Model

The most general Lagrangian for the decay $\mu \to eee$ can be written as [9]:

$$\begin{aligned} L_{\mu\to eee} \;=\; & \frac{4G_F}{2}\Big[m_\mu A_R \overline{\mu_R}\sigma^{\mu\nu} e_L F_{\mu\nu} + m_\mu A_L \overline{\mu_L}\sigma^{\mu\nu} e_R F_{\mu\nu} \\ & + g_1\,(\overline{\mu_R} e_L)\,(\overline{e_R} e_L) + g_2\,(\overline{\mu_L} e_R)\,(\overline{e_L} e_R) \\ & + g_3\,(\overline{\mu_R}\gamma^\mu e_R)\,(\overline{e_R}\gamma_\mu e_R) + g_4\,(\overline{\mu_L}\gamma^\mu e_L)\,(\overline{e_L}\gamma_\mu e_L) \\ & + g_5\;(\overline{\mu_R}\gamma^\mu e_R)\,(\overline{e_L}\gamma_\mu e_L) + g_6\,(\overline{\mu_L}\gamma^\mu e_L)\,(\overline{e_R}\gamma_\mu e_R) \;+\; H.c.\Big] \end{aligned} \tag{1}$$

This effective Lagrangian describes the tensor type LFV loops (dipole couplings) as shown in figure 1 b) and effective four-fermion contact interactions as shown in figure 1 c). The LFV dipole couplings are for instance tested in the radiative LFV muon decay $\mu \to e\gamma$. Loop diagrams with a virtual photon and four-fermion interactions can be tested in the decay $\mu \to eee$, demonstrating the complementarity of the two experiments.

In this effective model the kinematic properties of the decay, neglecting polarization effects, can be described by five coefficient functions:

$$\frac{d^4B(\mu \to eee)}{dx_1\; dx_2\; d\cos\theta\; d\phi} \;=\; \sum_{k=1}^{5} c_k\;\alpha_k(x_1, x_2) \tag{2}$$

The functions α_k are given in the appendix of [9]. The variables x_1 and x_2 are normalized energies of the more energetic and less energetic same charge decay lepton, respectively.

The coefficients c_k depend on the dipole couplings A and four-fermion couplings g_i in the following manner:

$$c_1 \;=\; g_{12}^2/16 + g_{34}^2 \tag{3}$$
$$c_2 \;=\; g_{56}^2 \tag{4}$$
$$c_3 \;=\; e\,A^2 \tag{5}$$
$$c_4 \;=\; e\,A g_{34}\,\eta \tag{6}$$
$$c_5 \;=\; e\,A g_{56}\,\eta' \tag{7}$$

where the following new definitions were used:

$$\begin{aligned} A^2 &= A_L^2 + A_R^2\,, \quad \tan\delta_0 = A_L/A_R \\ g_{12}^2 &= g_1^2 + g_2^2 \\ g_{34}^2 &= g_3^2 + g_4^2\,, \quad \tan\delta_{34} = g_3/g_4 \\ g_{56}^2 &= g_5^2 + g_6^2\,, \quad \tan\delta_{56} = g_5/g_6 \\ \eta &= \sin\delta_0 \sin\delta_{34} \sin\omega_3 + \cos\delta_0 \cos\delta_{34} \cos\omega_4 \\ \eta' &= \sin\delta_0 \sin\delta_{56} \sin\omega_5 + \cos\delta_0 \cos\delta_{56} \cos\omega_6 \end{aligned} \tag{8}$$

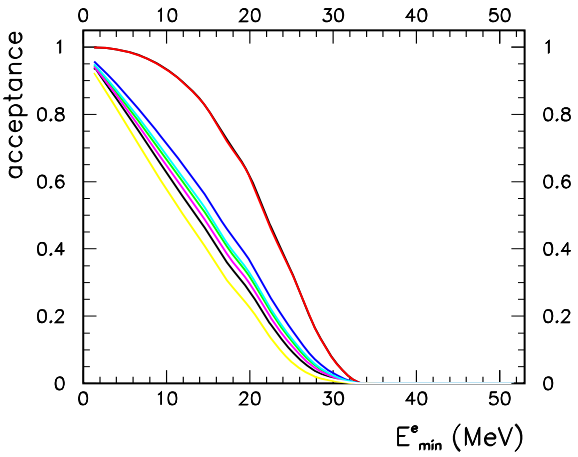

Figure 2: Energy distribution of the highest energy positron for different effective LFV models. The upper to lines, the red and the (almost hidden) black line, correspond to pure four-fermion contact interaction models (no penguin) contribution.

With the above notation the kinematic distribution of the decay can be essentially described by six parameters: g_{12}, g_{34}, g_{56}, A, η, η'. The parameter A describes the amplitude of the dipole coupling. The off-shell photon form factors contribute also to the terms g_3 - g_6 and can only be tested in $\mu \to eee$ decays. Scalar four-fermion couplings contribute to the parameters g_1 and g_2, whereas vector type four-fermion couplings contribute to g_3 - g_6. Terms containing the coefficients c_4 and c_5 are T-odd and describe interference effects between dipole and four-fermion couplings. They contribute only if both, LFV dipole couplings (loop) and LFV four-fermion couplings are present.

In case of a dominating on-shell dipole coupling ($|A| \gg |g_i|$) a quasi model independent relation between the $\mu \to eee$ decay rate and the $\mu \to e\gamma$ decay rate can be derived:

$$\frac{B(\mu \to eee)}{B(\mu \to e\gamma)} \approx 0.006 \tag{9}$$

In such models the decay $\mu \to eee$ has, compared to $\mu \to e\gamma$, a by two orders of magnitude lower sensitivity to the coupling A.

2.1. Model Dependence

The decay distributions of the three electron final state are model dependent. The kinematic acceptance of the detector is given by the decay electron[1] with lowest momentum, which is related to the bending radius of the reconstructed track and therefore with the strength of the magnetic field.

In figure 2 the acceptance is shown for different coefficient functions $a_k(x_1, x_2)$ (eq. 2) and their combinations as function of the minimum electron energy. The acceptances were calculate by typically setting one of the model parameters in equations 3-7 to one and all others to zero. The coefficient function $a_4(x_1, x_2)$ and $a_5(x_1, x_2)$ represent interference terms of dipole and four-fermion couplings. The influence of these terms is studied by evaluating the acceptance for different interference phases. It can be seen that all models with dipole couplings have a significantly lower acceptance than those with no dipole couplings (red and black line) and that with a low energy threshold of 15 MeV already half of the events are lost in LFV models with dominant dipole contributions. Therefore a low momentum threshold is an important design goal for the proposed experiment.

[1] the name electron is used in the following for both electrons and positrons if not stated otherwise.

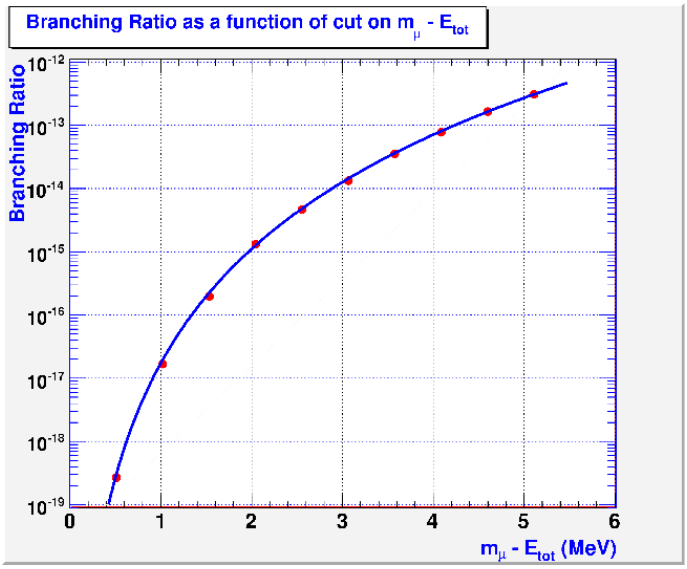

Figure 3: Branching ratio of the $\mu^+ \to e^+e^-(e^+)\nu\nu$ background process as function of the missing energy taken by the neutrinos. This plot is taken from [10].

2.2. Background Processes

The decay $\mu \to eee$ can be mimicked either by physics background processes like $\mu \to eee\nu\nu$, where the two neutrinos carry only very little energy or by accidental background. The process $\mu \to eee\nu\nu$ is called radiative muon decay with internal conversion and has the same signature as a radiative muon decay where the photon converts already in the target material. The internal conversion process constitutes an irreducible background, which crucially depends on the total energy resolution of the detector. The missing energy distribution from the two neutrinos of this process was calculated in [10] and is shown in figure 3. It can be seen that an absolute energy resolution of 1 MeV or better is required to suppress this background below a branching ratio of 10^{-16}. The very steep rise of the branching ratio as function of the missing energy suggests that already a small worsening of the energy resolution has a significant impact on this background.

For a beam of positive muons (μ^+) accidental background arises if background electrons (e^-) overlayed with positrons from ordinary muon decays mimic the $\mu \to eee$ decay. These electrons might be fake (e.g. wrongly reconstructed positrons), originate from converted photons or originate from Bhabha scattering if positrons interact with detector material (e.g. δ-electrons). This accidental background can be largely reduced by exploiting precise timing information, vertex information and kinematic constraints. For the latter a good spatial resolution of the detector is important as the vectors of the decay electrons all have to lie in a plane. The accidental background also increases with higher beam intensities. Therefore the usage of a DC beam is preferred over a pulsed muon beam.

3. Proposed Experiment

The detector concept of the proposed experiment is similar to the Sindrum experiment [5], performed more than 20 years ago: a continuous beam of surface anti-muons μ^+ of momentum $p = 28$ MeV/c are stopped on a hollow double-cone target of thin low Z-material. Decay electrons are detected in a multi-layer tracking detector, which is placed in a strong magnetic field for momentum measurement. The detector is completed by a system of fiber hodoscopes for precise timing measurements.

3.1. Beam and Target

The surface of the target should be large compared to the vertex resolution in order to resolve the different decay vertices of ordinary muon decays, see figure 4. Furthermore the opening angle of the cone should be small in order to

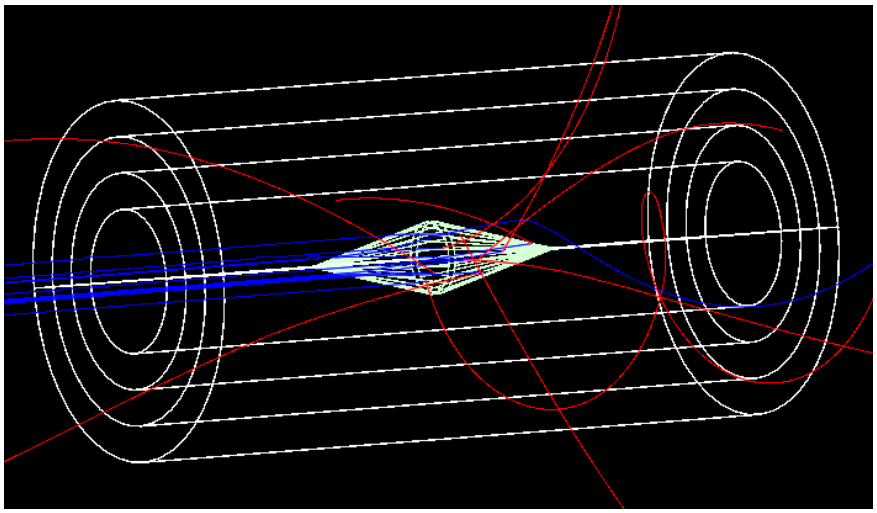

Figure 4: Simulation of ten muon decays using a simple detector geometry with four concentric layers of silicon sensors. The blue trajectories represent muons, which are stopped in the hollow double cone target, and the red trajectories decay electrons, which are bend in a solenoidal magnetic field.

minimize the target material in the transverse projection of decaying electrons while keeping a high stopping rate for muons (long stopping length). GEANT4 [11] simulations have shown that for a target of 2 cm diameter and length 7.6 cm an aluminum foil of thickness $\approx 60\,\mu$m gives a high muon stopping efficiency of more than 90%. Alternatively, also kapton$^{@}$ (polyimide) or other low Z materials could be considered for the target.

3.2. Tracking Detector

Most challenging is the design of the tracking detector, which must provide high spatial resolution for precise track and vertex reconstruction, and which therefore has to have a very small thickness of less than 100 μm to reduce multiple scattering. In the energy range of interest (15-53 MeV) multiple scattering effects dominate the momentum measurement and have direct impact on the total energy resolution. Compared to the previous Sindrum experiment [5] the tracking resolution in terms of track angular and momentum resolution has to improve by a factor of about five to achieve a sensitivity of 10^{-16}. In addition the tracking detector has to be capable of sustaining high rates. For the aimed sensitivity about 10^9 muon stops per second are required resulting in a similar particle rate in the detector. Gaseous detectors like drift chambers or proportional chambers might suffer from aging effects in such a high track multiplicity environment while silicon detectors are proven to be much more robust.

The above requirements are considered to be best fulfilled by using thin silicon pixel detectors, which can have thicknesses as small as 50 μm. Thin silicon detectors have been realized using the DEPFET technology [12, 13], developed for the future international linear collider detector and now being used as pixel detector for the Super-Belle upgrade, or by using the MAPS (monolithic active pixel sensor) technology [14, 15]. The MAPS technology has the nice feature of integrating the hit finding and readout electronics already in the sensor itself. This has the advantage of avoiding additional material due to readout chips, bump bondings, etc.. In addition MAPS can be produced in a relatively cheap standard CMOS process.

Both technologies have timing limitations due to the used frame readout (DEPFET) or due to the slow diffusion process in the charge collection (MAPS). These timing limitations are much less severe for the recently developed high voltage MAPS technology (also called ”smart diode array” - SDA) [16] with fast active charge collection. Therefore this technology is considered as base technology for the proposed $\mu \rightarrow eee$ experiment in the following.

3.2.1. High Voltage MAPS Technology

The schematic concept of the high voltage MAPS technology, developed by [16], is shown in figure 5. In contrast to the standard MAPS technology, where the charges are collected by diffusion, a strong electrical field in a small

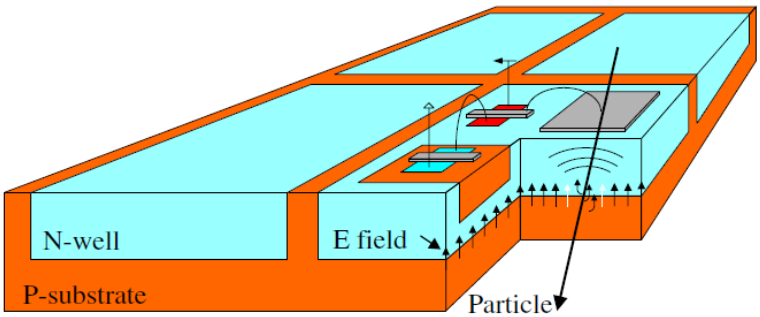

Figure 5: Sketch of the MAPS detector design from [16].

depletion zone (P-N junction) leads to a fast drift of the charge carriers. The CMOS transistors used to implement internal electronics of the chip are fully integrated in the N-well. This design offers a high signal to noise ratio, a fill factor of hundred percent and allows for small pixel sizes of 50 μm $\times$ 50 μm or even smaller [17, 18]. The hit detection and digitization are performed for each pixel cell simultaneously at high rate. The hit signals are processed in a large digital block placed on the sensor periphery for further readout. The on-detector hit detection and zero suppression saves resources and allows for a low material budget.

Another key feature of this technology is the possibility to thin down the thickness of the sensor. The transistor logic has a thickness of about 20 μm, which together with the depletion zone of about 10 μm allows for a sensor thickness as small as 40 – 50 μm. The mechanical stability of this thin sensors is critical and therefore first studies on system integration aspects including cooling were started.

For the planned experiment we consider a design with 80 μm $\times$ 80 μm pixel size[2] and a sensor thickness of 40 – 50 μm, corresponding to about 0.5 permil radiation length. For the thinning of the P-substrate standard industrial grinding techniques are considered to be used. The hit information can be readout at 10 MHz for which a power consumption of about 100mW per cm^2 of active sensor area is expected [19] (AMS HV 0.35 μm technology). By combining and connecting three chips the total sensor geometry could be 60×10 mm^2 for the inner and 60×20 mm^2 for the outer detector layers. The data bandwidth depends mainly on the distance between the sensor and the target. For a distance of 10 mm and $10^9/s$ muon stops the occupancy of a pixel cell is about 10^{-4} per clock cycle. The resulting bandwidth of about 800 MBit/s can be readout by a single LVDS link per sensor.

3.3. Fiber Tracker

As the silicon tracker provides timing information of hits in 100 ns intervals, in average about 100 muon decays are recorded per clock cycle. In order to reduce the accidental background a timing resolution of 0.1 ns is aimed for. This can be achieved with an additional tracking system consisting of scintillating fibers and fast photon detectors. A similar system was recently successfully used by a balloon-borne detector experiment [20]. This system can be placed either outside or inside the silicon detector.

The proposed outer fiber tracker consists of concentrical layers of scintillating fibers with a diameter of 0.25-1.0 mm. Scintillating light is detected by fast silicon photomultiplers (SiPM) at both ends and digitized with an expected timing resolution of 50 – 60 ps. This timing resolution is achievable if at least ten photons are detected per SiPM, which is expected to be the case for 0.25 mm fibers with double sided readout. SiPMs are ideal devices for detecting light from a scintillating fiber detector because of their compactness, high gain of 10^5-10^6 and their insensitivity to magnetic fields.

By measuring the timing difference between the signals arriving at both wire ends, also the longitudinal hit position can be measured with a resolution of about 1.0 cm. The azimuthal hit position is given by the scintillating

[2] this size corresponds to about 50% of the resolution from multiple scattering alone.

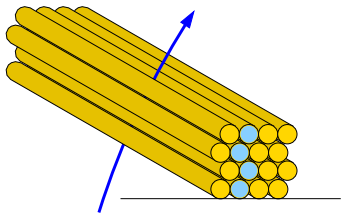

Figure 6: Sketch of a fiber tracker hodoscope using several layers of scintillating fibers

fiber diameter. If several layers of scintillating fibers are overlayed also the inclination angle in the transverse plane (azimuthal angle) can be measured, see figure 6.

The total number of readout channels is about 2 $\times$ 5000 using scintillating fibers with a diameter of 1.0 mm at a radius of 10 cm. The average hit rate for 10^9 muon stops per second is about 1 MHz per fiber, which is small compared to the SiPM signal length of about 2 ns. An inner scintillating fiber placed at a smaller distance from the target should have thinner fibers (e.g. 0.25 mm) to keep the occupancy low. Also multiple scattering is a critical issue and the material budget has to be kept low as well.

3.4. Detector Geometry

For the proposed experiment the single hit resolution is about a factor two smaller than the effect from multiple scattering. In contrast to tracking detectors with dominating hit resolution error, in the case of dominating multiple scattering effects the number of detector layers should not be larger than three or four as the track resolution degrades with the square root of the number of layers. For redundancy reasons we consider four layers optimal.

A complication comes from the fact that tracks have to be measured over a large momentum range (15-53 MeV/c) and that the optimal track resolution depends on the lever arm between the first to the last layer. Because of the different bending radii of tracks in the momentum interval of interest a compromise has to be chosen. The momentum of a track is determined by its bending in a magnetic field. For dominating multiple scattering the absolute momentum resolution scales linearly with the momentum ($\sigma_p/p = const$).

Using a solenoidal magnetic field and four layers, the momentum resolution in a multiple scattering environment is approximately given by:

$$\frac{\sigma_p}{p} \approx 2\,\frac{b}{BL} \quad , \tag{10}$$

with $b = 0.001$ Tm for silicon layers of 40 μm thickness, B the strength of the axial magnetic field and L the radial distance between the first and the last layer [3]. As high momentum tracks (large bending radius) contribute with a large weight to the total energy measurement, a design is proposed, which measures high momentum tracks at $p_T > 20$ MeV using four silicon layers with a large lever arm, and lower momentum tracks at $p_T < 20$ MeV using only three layers, see figure 7.

To allow for precise timing measurements of low momentum tracks, a thin inner fiber tracker at small radius, see figure 7, could complement an outer fiber tracker. Because of multiple scattering the inner fiber detector should not consist of more than 2 layers of 0.25 mm fibers.

For the geometry shown in figure 7 the momentum resolution of transverse decay electrons is calculated as $\sigma_{p_T} =$ 0.60 (0.46) MeV/c at $p = 50$ (20) MeV/c in a magnetic field of $B = 1.4$ T using the silicon layers only. These values include multiple scattering in the silicon but ignore multiple scattering in an optional inner fiber tracker. However, even if this additional material is taken into account, the resolution is expected to improve if a broken line fit [21] is used and a vertex constraint is applied in the track fit. A considerable improvement is also expected if the trajectory of the returning electron after the curl is measured and combined with the measurement of the first track half. In summary, a total energy resolution of about $E = 1$ MeV/c or better is expected.

[3] non-linear effects due to the bending are neglected.

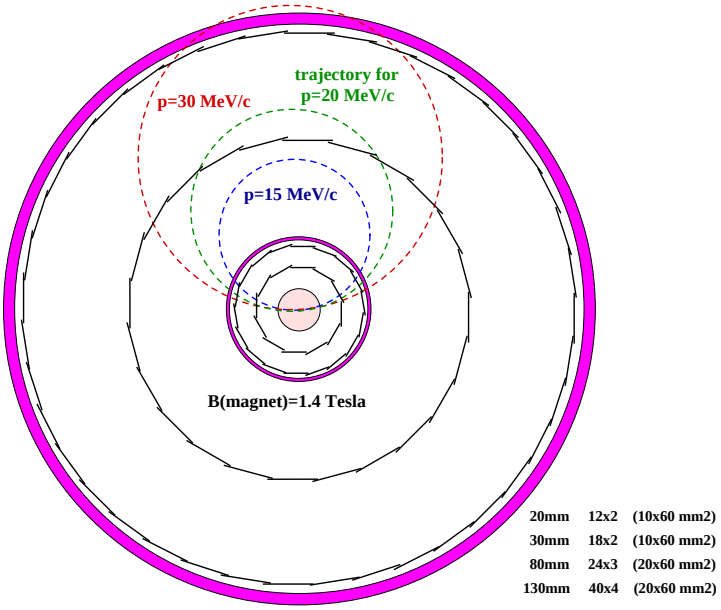

Figure 7: Radial view of the proposed detector consisting of four layers of pixel sensors (black) and two fiber trackers (pink). For illustration trajectories of electrons with 15, 20 and 30 MeV are indicated using a axial magnetic field of 1.4 T.

3.5. Readout and Data Acquisition

For a four layer design with about 50 million pixels and 5000 scintillating fibers the total bandwidth is estimated to be 16 GByte/s for a muon stop rate of 10^9 muons per second. The front-end electronics should provide digitization, hit finding and zero suppression. The resulting data rate can then be readout using high speed data links without the need of any hardware trigger and then processed by an online filter farm, which provides a reconstruction of all electron tracks, searches for decay electrons (e^-), looks for common decay vertices, timing coincidences and finally selects $\mu \to eee$ candidates.

4. Simulation Results

First simulation studies for a simple detector geometry were performed using the GEANT4 program [11]. The goal was to study possible confusion problems (hit ambiguities) in the track reconstruction and to check the influence of multiple scattering on the track reconstruction and track parameter resolution.

For these studies a simple geometry is used: a hollow double cone target of 7.6 cm length and a maximum diameter of 2 cm, four equidistant layers at radii 2, 3, 4 and 5 cm, and a magnetic field of 1 Tesla. The effect of recording in average 100 muon decays per 100 ns clock cycle (for 10^9 muon stops per second) is shown in figure 8. Studies indicate that all trajectories of up to 100 electrons in the geometric acceptance of the detector can be unambiguously reconstructed and that the reconstructed track parameter resolution is described by equation 10.

The vertex resolution was found with this geometry to be $\sigma_{vtx} = 150\,\mu$m and the polar angle[4] resolution was found to be 5 mrad. These resolutions depend mainly on the amount of multiple scattering in the first silicon layer (thickness of 50 μm was assumed here) and are basically independent of the details of the detector geometry. In contrast, the momentum and the azimuthal angle resolution are highly correlated and depend strongly on the detector geometry and are subject of further studies.

[4] angle orthogonal to the bending plane

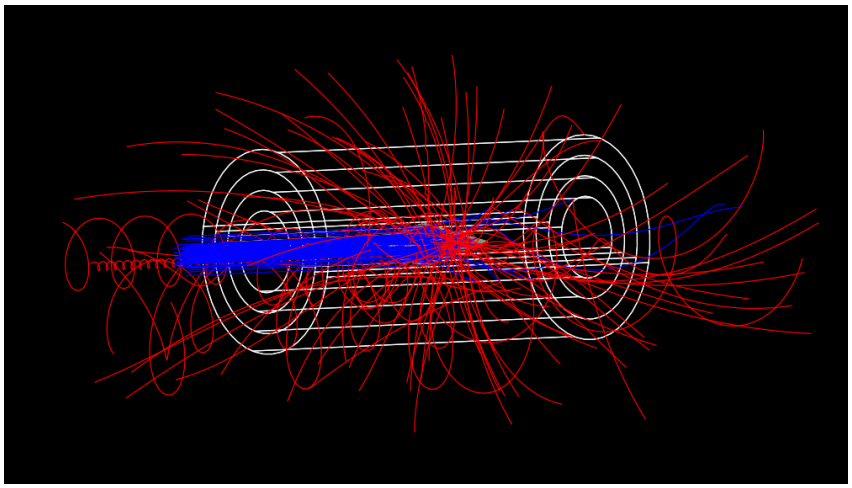

Figure 8: Overlay of one hundred simulated muon decays as recorded by the pixel detector in a time frame of 100 ns. For details see figure 4

4.1. Accidental Backgrounds

Two accidental background processes were studied with background Monte Carlos programs, which implement the matrix element for the ordinary muon decay (Michel spectrum) and the radiative muon decay with internal conversion [10]:

- accidental coincidences of two muon decays (yielding two positrons) and the occurrence of a fake electron track, which could either originate from wrong reconstruction, from a not identified back-curling positron or from Bhabha scattering,
- accidental coincidences of a radiative muon decay with internal conversion where one electron is not detected, $\mu^+ \to e^+e^-(e^-)\nu\nu$, and an ordinary muon decay.

For both cases the backgrounds were found to be negligible ($\ll 10^{-16}$) if the total energy resolution is better than 3 MeV, the timing resolution is 0.1 ns and the probability to find a fake electron track is below 10% per muon decay[5]. This large background rejection was achieved by exploiting kinematic, timing and vertex constraints.

4.2. Physics Background

The most relevant background, the radiative muon decay with internal conversion, was also studied with a Monte Carlo generator for varying energy resolutions. The result is shown in figure 9, where the background rate is shown as function of the total energy resolution for different search window cuts. It can be seen that the search sensitivity depends crucially on the energy resolution and the size of the search window. For the aimed sensitivity of 10^{-16} and a 2σ search window cut (95% acceptance) an energy resolution of 0.6 MeV would be required. This sensitivity is in the reach of the proposed experiment, if improved fitting techniques (e.g. broken line fit) and vertex constraint fits are used, and if back-curling track halfs are also measured.

5. Conclusions

A new experiment to search for the LFV decay $\mu \to eee$ using thinned silicon pixel sensors as tracking detector has been proposed. These sensors could be as thin as 40-50 μm and would provide precise hit information at 0.5 permil radiation length per layer.

[5] a flat momentum distribution was assumed here.

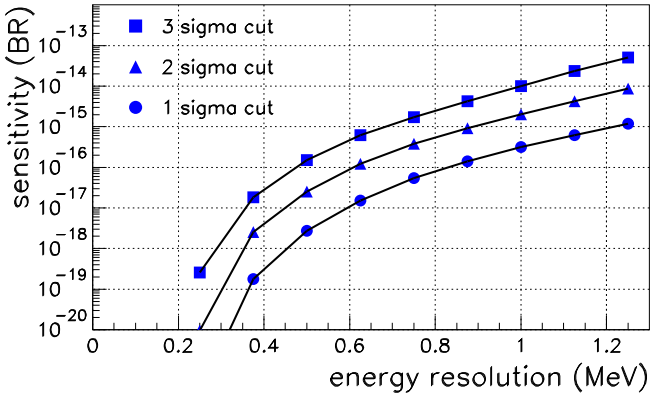

Figure 9: Simulated background rate as function of the total energy resolution for different search window cuts (1σ, 2σ, 3σ) with respect to the energy resolution.

This experiment performed at an upgraded or new beam-line at the Paul-Scherrer Institute (Switzerland) could achieve a sensitivity to branching ratios as small as B($\mu \rightarrow eee$)=10^{-16}, which would test new physics models with unprecedented sensitivity beyond the reach of previous or running experiments.

The process $\mu \rightarrow eee$ is complementary to other LFV searches at low energies ($\mu \rightarrow e\gamma$ or $\mu \rightarrow e$ conversion) and tests also physics beyond the Standard Model at a mass scale much higher than accessible by LHC experiments.

6. Acknowledgments

We would like to thank the organizers of this workshop for their kind hospitality and for providing an environment with many interesting and fruitful discussions. A.S. wants to thank Peter Fischer and Ivan Peric for imparting knowledge on MAPS technology aspects and Stefan Ritt and Klaus Kirch for motivating this design study.

7. References

[1] L. Brooks *et al.*, (MEGA Collaboration), Phys. Rev. Lett. 83, 1521 (1999).
[2] D. Nicolo *et al.*, MEG Collaboration, Nucl. Instrum. Meth. A **503** (2003) 287.
[3] J.Adam *et al.*, Nuclear Physics B Volume 834, Issues 1-2, (2010) 1.
[4] T. Iwamoto *et al.*, MEG Collaboration, talk presented at the ICHEP conference 2010, Paris.
[5] U. Bellgardt, et al., Nucl. Phys. B 229, (1988) 1.
[6] J. Kaulard *et al.*, Sindrum II Collaboration, Phys. Lett. B **422** (1998) 334.
[7] B. Aubert *et al.*, Babar Collaboration, Phys. Rev. Lett. 104 021802 (2010).
[8] Y. Miyazaki *et al.*, Belle Collaboration, Phys. Lett. B 682 (2010) 355.
[9] Y. Kuno and Y. Okada, Rev. Mod. Phys.73 (2001) 151 arXiv:hep-ph/9909265.
[10] R.M. Djilkibaev and R.V. Konoplich, Physics Review D79 073004 (2009).
[11] GEANT4 programm, Nucl. Instr. and Meth. A 506 (2003) 250-303.
[12] P. Fischer *et al.*, Nucl. Instrum. Meth. A **582** (2007) 843.
[13] L. Andricek *et al.*, Nucl. Instrum. Meth. A **565** (2006) 165.
[14] G. Gaycken *et al.*, Nucl. Instrum. Meth. A **560** (2006) 44.
[15] C. Hu-Guo *et al.*, JINST **4**, P04012 (2009).
[16] I.Perić, Nucl.Instr. and Meth.A 582 (2007) 876885.
[17] I.Perić , C.Takacs, Nucl.Instr.and Meth.A(2010),doi:10.1016/j.nima.2010.03.161.
[18] I.Perić *et. al.*, Nucl.Instr. and Meth.A(2010),doi:10.1016/j.nima.2010.06.337.
[19] I.Perić, design note, unpublished.
[20] B. Beischer *et al.*, Nucl. Instr. and Meth. A 622 (2010) 542-544.
[21] V. Blobel, Nucl. Instr. Meth. A 566 (2006) 14.